Temporal Changes in Immune Responses within the Tumor Microenvironment in the 4T1.2-HER2 Mammary Tumor Model

Yitong Xu
Penn State: The Pennsylvania State University
Connie Rogers (cjr102@psu.edu)
Pennsylvania State University University Park : Penn State https://orcid.org/0000-0003-4072-2721

Research article

Keywords: breast cancer, immunogenicity, HER2 antigen, antigen-specific immune response, TILs

Posted Date: February 9th, 2021

DOI: https://doi.org/10.21203/rs.3.rs-180530/v1

Abstract

Background: The murine 4T1.2 triple-negative breast cancer model is widely used, but is poorly immunogenic with no defined tumor-associated antigens. A modified 4T1.2 model has been developed that stably expresses a surrogate tumor antigen, human epidermal growth factor receptor-2 (HER2). The goal of the current study was to characterize host immune responses in the 4T1.2-HER2 tumor model, focusing on the tumor microenvironment (TME) during the early stage of tumor development.

Methods: Female BALB/c mice were orthotopically inoculated with 4T1.2-HER2 tumor cells and sacrificed at day (D) 6, 9, 12, 15 and 18 post tumor inoculation. The phenotype and function of tumor-infiltrating immune cells were assessed.

Results: 4T1.2 and 4T1.2-HER2 tumor cells had similar proliferation rates *in vitro*. In contrast to the rapid progression of the parental 4T1.2 model, the 4T1.2-HER2 model demonstrated initial tumor growth followed by spontaneous tumor regression by D18 post tumor inoculation, which was not observed in *scid* mice. Following tumor regression, mice demonstrated either a second phase of tumor outgrowth or complete tumor rejection. Within the TME, the percentage of T cells was reduced at D9 and increased during tumor regression through D18 ($p<0.05$), whereas the percentage of myeloid-derived suppressor cells (MDSCs) increased during the initial tumor growth and was reduced by D18 ($p<0.01$). There was a stepwise increase in the percentage of $IFNg^+$, $IL\text{-}2^+$ and $perforin^+$ T cells and NK cells peaking at D12-15. Furthermore, tumor regression occurred concurrently with HER2-specific IFNg production from tumor-infiltrating immune cells at D12 and D15 ($p<0.05$). During the second phase of 4T1.2-HER2 tumor growth, tumor volume was negatively correlated with immune infiltration ($r=0.662$, $p=0.052$).

Conclusions: These results suggest that the integration of a surrogate tumor antigen, human HER2, into the clinically relevant, yet poorly immunogenic 4T1.2 breast cancer model enhanced its immunogenicity and induced HER2-specific immune responses.

Background

Breast cancer is the most commonly diagnosed cancer and one of the leading causes of death among women worldwide (1). The role of immune system in cancer control is well established and is achieved by a wide variety of anti-tumor mediators. $CD8^+$ cytotoxic T cells (CTLs) and natural killer (NK) cells are primarily responsible for the killing of transformed cells, whereas $CD4^+$ helper T cells orchestrate diverse immune responses by producing cytokines such as IFNγ (2, 3). As tumor progression occurs, however, immunosuppressive cells from both the myeloid [myeloid-derived suppressor cells (MDSCs)] and lymphoid [regulatory T cells (Tregs)] lineages are also induced and recruited to the tumor microenvironment (TME) to facilitate immune escape (2–5). The TME can be broadly categorized into “hot” or “cold” based on immune infiltration, which is closely related to prognosis and therapeutic efficacy (6–8). Breast cancer is traditionally viewed as non-immunogenic with relatively low mutation rates and tumor-infiltrating lymphocyte (TIL) levels. However, among the heterogeneous breast cancer subtypes,

human epidermal growth factor receptor-2 (HER2)-positive and triple-negative breast cancer (TNBC) have higher levels of mutational burden and TIL infiltration compared to hormone receptor (HR)-positive breast cancer (9, 10). Moreover, higher TIL levels are associated with reduced risk of tumor recurrence and mortality in $HER2^+$ breast cancer and TNBC, and are predictive of response to neoadjuvant chemotherapy in all subtypes of breast cancer (11–14).

In recent years, significant clinical advances have been made in cancer immunotherapies. T cells have been the major focus of therapeutic efforts due to their capacity to specifically recognize tumor antigens derived from all cellular compartments, followed by direct killing of tumor cells and/or integration of various effector mechanisms (15). In particular, antibody blockade of immune checkpoints has demonstrated the most success in multiple cancer types including breast cancer (9, 16, 17). However, patient response rates to immune checkpoint blockade in most cancer types are limited to 10–25%, and a substantial percentage of patients eventually demonstrate disease progression after initial response to therapy for reasons that are not clearly understood (15, 18–20). Therefore, additional studies in preclinical cancer models that closely mimic human diseases are needed to better understand the mechanisms underlying cancer resistance to immunotherapies and to develop novel therapeutic strategies to improve clinical outcomes.

The 4T1.2 murine breast cancer model is a highly aggressive model of advanced TNBC. When the 4T1.2 tumor is inoculated orthotopically into the mammary fat pad, it spontaneously metastasizes to the lung and bone, two common sites of metastasis in breast cancer patients (21–23). Moreover, the use of this syngeneic model in immunocompetent hosts enables the study of the TME under the influence of an intact immune system. Despite its unique strength in mimicking human metastatic breast cancer, the 4T1.2 model is poorly immunogenic with no defined tumor-associated antigens (TAAs). This severely limits its utility in studying the effects and mechanisms of immunotherapeutic interventions on modulating antigen-specific immune responses.

One commonly used strategy to overcome the drawback of poorly immunogenic tumor models is by introducing surrogate tumor antigens into the tumor cells (24–27). HER2 (rodent homolog neu) is a TAA that is overexpressed in several cancer types, including in 25–30% of human breast cancers (28). Several murine cancer cell lines expressing the human HER2 antigen have been established and demonstrate robust immune responses against a well-defined H-$2K^d$-restricted HER2 epitope (26, 29–31). In particular, 4T1.2 cells expressing human HER2 (4T1.2-HER2) are shown to induce HER2-specific IFNγ production and CTL activity when inoculated subcutaneously (s.c.) in immunocompetent BALB/c mice (26). Moreover, s.c. 4T1.2-HER2 tumor growth demonstrates a spontaneous regression period which is dependent on $CD8^+$ T cells (26). These data suggest that the addition of human HER2 protein to the 4T1.2 tumor may enhance its immunogenicity and thus enable the study of antigen-specific immune responses in this clinically relevant breast cancer model. However, previous data on host immune responses in the 4T1.2-HER2 model in immunocompetent mice are limited, and are based on s.c. 4T1.2-HER2 tumor model which may not represent the mammary tissue environment in human breast cancer (26). Therefore, the goal of the current study was to characterize host immune responses in the

orthotopic (intramammary inoculation) 4T1.2-HER2 tumor model, focusing on the TME during the early stage of tumor development.

Methods

In vitro**characterization of tumor cell lines**

Cell lines and cell culture

4T1.2-HER2 and the parental 4T1.2 murine breast cancer cell lines were kindly provided by Dr. Phillip Darcy (Peter MacCallum Cancer Centre, East Melbourne, Victoria, Australia) and maintained in DMEM (Life Technologies, Grand Island, NY) supplemented with 10% fetal bovine serum (Gemini Bio-Products, Sacramento, CA), 2 mM L-glutamine (Mediatech, Manassas, VA) and 1% penicillin/streptomycin (Mediatech). P815 cells were purchased from ATCC (Manassas, VA) and maintained in complete medium [RPMI 1640 (Mediatech) supplemented with 10% fetal bovine serum, 2 mM L-glutamine, 1X nonessential amino acids (Mediatech), 1 mM sodium pyruvate (Mediatech), 10 mM HEPES buffer (Mediatech), 1% penicillin/streptomycin, and 50 μM β-mercaptoethanol (Gibco, Grand Island, NY)]. All cell lines were cultured at 37°C with 5% CO_2.

In vitro cell proliferation assay

Serial dilutions of 4T1.2 and 4T1.2-HER2 cells were cultured in 96-well plates in triplicates for 72h. CellTiter 96® AQueous One Solution Reagent (MTS) (Promega, Madison, WI) was added (20 μl/well) at 71h and incubated with the cells for one hour. Absorbance was measured at 490nm using an Epoch™ Microplate Spectrophotometer (BioTek, Winooski, VT).

Flow cytometric analyses of tumor cell lines

Cultured 4T1.2 and 4T1.2-HER2 cells were trypsinized and washed with PBS containing 0.1% bovine serum albumin (BSA) at 4°C. Cells were incubated with Fc block (BioLegend, San Diego, CA) and stained with fluorescent dye-conjugated antibodies (**Additional File 1: Table S1**) or the corresponding isotype control antibodies for 30 min at 4°C. Following antibody incubation, cells were washed twice and fixed with BD Cytofix™ fixation buffer (BD Biosciences). All flow cytometric analyses were performed on a BD LSR-Fortessa (BD Biosciences) flow cytometer. Data analyses were preformed using FlowJo V10 (Tree Star, Ashland, OR).

Animal model

Female BALB/c and BALB/c *scid* mice were purchased from Jackson Laboratory (Bar Harbor, MA). In one experiment, BALB/c mice were orthotopically inoculated with $5x10^4$ 4T1.2 cells or $2x10^6$ 4T1.2-HER2 cells (n = 4–5/group) into the fourth mammary fat pad to compare tumor growth patterns in the 4T1.2 vs. 4T1.2-HER2 model. Additionally, BALB/c *scid* mice (n = 5) were orthotopically inoculated with $5x10^5$ 4T1.2 HER2 cells to evaluate the role of the adaptive immune system in regulating 4T1.2-HER2 tumor

growth. In a second experiment, BALB/c mice were orthotopically inoculated with $2x10^6$ 4T1.2-HER2 cells and sacrificed at day 6, 9, 12, 15 and 18 post tumor inoculation (n = 8/time point) to evaluate immune outcomes during the early stage of 4T1.2-HER2 tumor development. In a third experiment, BALB/c mice were orthotopically inoculated with $5x10^5$, $1x10^6$ or $2x10^6$ 4T1.2 HER2 cells (n = 4–5/group) and sacrificed between day 44–64 post tumor inoculation to evaluate tumor recurrence and immune outcomes during the second phase of tumor growth or tumor rejection. Primary tumor growth was measured three times/week using a digital caliper, and tumor volume was calculated following the equation $V=(short^2 \times long)/2$. All mice were housed at the Pennsylvania State University and maintained on a 12-hour light/dark cycle with free access to AIN-76A diet (Research Diets, New Brunswick, NJ) and water. The Institutional Animal Care and Use Committee of the Pennsylvania State University approved all animal experiments.

Isolation of splenic and tumor-infiltrating immune cells

At sacrifice, spleens and tumors were harvested and single cell suspensions of splenocytes and tumor-infiltrating immune cells were prepared as previously described (23). Briefly, spleens were mechanically disrupted with a syringe plunger and passed through a 70 μm nylon mesh strainer. Primary tumors were weighed, minced into fine pieces and incubated with 0.03 mg/mL Liberase (Roche, Indianapolis, IN) and 12.5 U/mL DNase I (Thermo Fisher Scientific, Waltham, MA) for 45 min at 37°C on a rotary sample mixer. Following the digestion, remaining pieces were mechanically disrupted with a syringe plunger and passed through a 70 μm nylon mesh strainer. Following mechanical disruption, both spleen and tumor samples were treated with ACK lysing buffer (Lonza, Basel, Switzerland), washed and resuspended in complete medium. Cell counts and viability were determined via trypan blue (Mediatech) exclusion.

Immune cell assays

Flow cytometric analyses of myeloid and lymphoid cells

Single cell suspensions of splenocytes and tumor-infiltrating immune cells were washed with PBS containing 0.1% BSA and incubated with Fc block (BioLegend), followed by staining with Zombie Aqua viability dye (BioLegend). Cells were then stained with fluorescent dye-conjugated antibodies against extracellular markers (**Additional File 1: Table S2**) or the corresponding isotype control antibodies for 30 min at 4°C. CD45 staining was used in each panel to identify total leukocytes. Following antibody incubation, cells were washed twice and fixed with BD Cytofix™ fixation buffer (BD Biosciences). Additionally, regulatory T cells (Tregs) were assessed using the Mouse Regulatory T Cell Staining Kit (eBioscience) as per manufacturer's instructions. Following extracellular staining for CD4 and CD25, cells were incubated in a Fixation/Permeabilization solution for 30 min, washed twice, and stained with FoxP3 antibody (**Additional File 1: Table S2**) or the corresponding isotype control antibody for 30 min. After intracellular staining, cells were washed twice and samples were analyzed with the flow cytometer within 12h.

Flow cytometric analyses of effector molecules

Splenocytes and tumor-infiltrating immune cells were incubated with 10 µg/mL brefeldin A (BFA) or DMSO control (0.2% v/v) in complete medium for 4h at 37°C. Cells were then washed with PBS containing 0.1% BSA at 4°C and stained sequentially with Fc block, Zombie Aqua, and fluorescent dye-conjugated antibodies (**Additional File 1: Table S2**) or the corresponding isotype control antibodies as described above. The expression of effector molecules by splenic and tumor-infiltrating lymphoid cells was then assessed using BD Fixation/Permeabilization Solution Kit (BD Biosciences) as per manufacturer's instructions. Following extracellular staining for CD4, CD8 and CD49b, cells were incubated in a Fixation/Permeabilization solution for 20 min, washed twice, and stained with antibodies against IFNγ, IL-2, TNFα and perforin (**Additional File 1: Table S2**) or the corresponding isotype control antibodies for 30 min. After intracellular staining, cells were washed twice and samples were analyzed with the flow cytometer within 12h.

Antigen-specific IFNγ production

Splenocytes and tumor-infiltrating immune cells were cultured in 24-well plates ($1x10^6$ cells in 0.5 mL complete medium per well) in the presence of 10 µg/mL H-$2K^d$-restricted HER2 p63-71 peptide (TYLPTNASL; CPC Scientific, San Jose, CA) or influenza HA p518-526 peptide (IYSTVASSL; GenScript, Piscataway, NJ). Additionally, splenocytes stimulated with 1 µg/mL anti-CD3 (BD Biosciences) and tumor-infiltrating immune cells stimulated with 1 µg/mL anti-CD3 and anti-CD28 (BD Biosciences) were used as positive control. Splenocytes and tumor-infiltrating immune cells cultured without stimulus were used as negative control. After 48h, culture supernatants were collected and IFNγ secretion was measured using ELISA MAX™ Deluxe Set (BioLegend).

Statistical analyses

All data were assessed for normality and equal variances, and either parametric or nonparametric analyses were used to detect differences between groups. If data were skewed, log or square root transformation was done prior to statistical analyses. Differences in tumor weight, splenic and tumor-infiltrating immune cell number, and the composition of splenic and tumor-infiltrating immune cells between time points were assessed using one-way ANOVA or Kruskal-Wallis test, followed by Bonferroni or Dunn's multiple comparison test where appropriate. *In vitro* cell proliferation and the percentage of immune cells expressing effector molecules were examined using two-way ANOVA, followed by Bonferroni multiple comparison test where appropriate. IFNγ secretion in response to different stimuli at each time point was assessed using paired t test or Wilcoxon test. The relationship between tumor volume and the percentage of splenic and tumor-infiltrating immune cells was analyzed using Pearson correlation test. Differences in splenic effector to immunosuppressive cell ratios between tumor-free and tumor-bearing mice were assessed using Student's t test. All analyses were conducted using GraphPad Prism 7 (GraphPad Software, San Diego, CA). All data are presented as mean ± SEM. Statistical significance was accepted at $p \leq 0.05$.

Results

Expression of major histocompatibility complex (MHC) and costimulatory molecules in vitro **was not different between 4T1.2 and 4T1.2-HER2 tumor cell lines**

4T1.2-HER2 tumor cells expressed high levels of HER2 whereas 4T1.2 tumor cells were HER2-negative (**Additional File 2: Figure S1**). Both 4T1.2 and 4T1.2-HER2 cells were positive for MHC I molecules (H-2K^d and H-2D^d) and negative for MHC II (I-A^d) and costimulatory molecules (CD80 and CD86) (**Additional File 2: Figure S1**).

4T1.2 and 4T1.2-HER2 tumor cells had similar proliferation rates in vitro **but different tumor growth patterns** in vivo

4T1.2 and 4T1.2-HER2 tumor cells had similar *in vitro* proliferation rates (Fig. 1A). When inoculated orthotopically into wildtype BALB/c mice, 4T1.2 tumor ($5x10^4$ cells inoculated) demonstrated a rapid, continuous progression and mice became moribund at as early as day (D) 30 post tumor inoculation (Fig. 1B). Despite a 40-fold higher dose of tumor cell inoculation, 4T1.2-HER2 ($2x10^6$ cells inoculated) tumor development did not track the rapid progression as observed in the 4T1.2 model but consisted of three phases: (i) initial tumor growth, (ii) spontaneous tumor regression, and (iii) a second phase of tumor outgrowth or tumor rejection (Fig. 1C). In a separate experiment where mice were inoculated with different doses of 4T1.2-HER2 tumor cells, tumor recurrence rate during phase (iii) showed an increasing trend with increasing doses of tumor cell inoculation (χ^2 test for trend, $p = 0.076$). Additionally, when inoculated into immunodeficient BALB/c *scid* mice, 4T1.2-HER2 tumor ($5x10^5$ cells inoculated) demonstrated a rapid, continuous progression and no spontaneous tumor regression was observed (Fig. 1D).

4T1.2-HER2 tumor growth was associated with changes in tumor-infiltrating effector and immunosuppressive cells

Female BALB/c mice were orthotopically inoculated with $2x10^6$ 4T1.2-HER2 cells and sacrificed at D6, 9, 12, 15 and 18 post tumor inoculation (n = 8/time point). Initial tumor growth peaked at D9 and was followed by spontaneous tumor regression (Fig. 2A). There was a significant difference in terminal tumor weight (Fig. 2B) (one-way ANOVA, $F(4, 22) = 3.167$, $p = 0.034$) and splenic cell number (Fig. 2C) (one-way ANOVA, $F(4, 35) = 2.692$, $p = 0.047$) across all time points. The number of total tumor-infiltrating immune cells (Fig. 2D) and infiltrating cells per gram of tumor (Fig. 2E) was not significantly different across all time points.

Among tumor-infiltrating effector cells, the percentage of tumor-infiltrating CD4$^+$ (Fig. 3A) (Kruskal-Wallis test, $KW = 14.35$, $p = 0.006$) and CD8$^+$ (Fig. 3B) (one-way ANOVA, $F(4, 22) = 3.35$, $p = 0.028$) T cells was reduced from D6 to D9 during the initial tumor growth period and increased after D9 as tumor regression occurred. The percentage of tumor-infiltrating CD49b$^+$ NK cells (Fig. 3C) (one-way ANOVA, $F(4, 20) = 55.01$, $p < 0.001$) was reduced at D9-18 compared to D6. In the immunosuppressive compartment, the percentage of tumor-infiltrating Gr-1$^+$/CD11b$^+$ MDSCs (Fig. 3D) (one-way ANOVA, $F(4, 22) = 4.962$, $p = 0.005$) was reduced at D18, CD11b$^+$/Ly6C^{lo}/Ly6G$^+$ gMDSCs (Fig. 3E) was unchanged, and

$CD11b^+/Ly6C^{hi}/Ly6G^-$ mMDSCs (Fig. 3F) (Kruskal-Wallis test, KW = 13.79, p = 0.008) was reduced over time. Tumor-infiltrating $CD4^+$:MDSC (Fig. 3G) (one-way ANOVA, F(4, 22) = 5.168, p = 0.004) and $CD8^+$:MDSC (Fig. 3H) (one-way ANOVA, F(4, 22) = 5.481, p = 0.003) ratios were increased at D18.

Splenic $CD4^+$ and $CD8^+$ T cells demonstrated the same trend with tumor-infiltrating T cells and was reduced from D6 to D9 and increased after D9 (**Additional File 2: Figure S2**). In contrast to T cells, splenic MDSCs were increased from D6 to D9 and reduced after D9. As a result, splenic $CD4^+$:MDSC and $CD8^+$:MDSC ratios were reduced from D6 to D9 during the initial tumor growth period and increased after D9 as tumor regression occurred (**Additional File 1: Figure S2**). The distribution of other myeloid cells and Tregs in the spleen and the tumor are shown in **Additional File 2: Figure S3** and **Additional File 2: Figure S4**, respectively.

4T1.2-HER2 tumor growth was associated with changes in tumor-infiltrating memory T cells

Within tumor-infiltrating T cells, the percentage of $CD44^+/CD62L^+$ central memory (T_{CM}) cells within $CD4^+$ (one-way ANOVA, F = 9.310, p < 0.001) and $CD8^+$ (one-way ANOVA, F = 4.510, p = 0.008) T cells was increased over time. The percentage of $CD44^+/CD62L^-$ effector memory (T_{EM}) cells within $CD4^+$ T cells was reduced at D15 compared to D6-9 (one-way ANOVA, F = 5.127, p = 0.005). The percentage of $CD69^+$, $CD25^+$, $CD44^-/CD62L^+$ naïve and $CD44^-/CD62L^-$ effector cells within tumor-infiltrating $CD4^+$ or $CD8^+$ T cells was not significantly different between time points (Table 1).

Table 1
Temporal changes in tumor-infiltrating activated and/or memory T cells during 4T1.2-HER2 tumor growth.

Tumor		D6	D9	D12	D15	D18	p-value
% of $CD4^+$ T cells	$CD69^+$	7.12 ± 0.78	8.66 ± 0.43	8.82 ± 0.41	7.74 ± 0.80	8.25 ± 0.69	0.301
	$CD25^+$	9.79 ± 0.46	10.9 ± 0.54	9.83 ± 0.25	10.2 ± 0.59	11.5 ± 0.13	0.117
	$CD44^-/CD62L^+$ (naïve)	85.9 ± 2.38	83.1 ± 1.59	85.0 ± 1.50	85.5 ± 2.36	86.9 ± 0.41	0.494
	$CD44^-/CD62L^-$ (effector)	7.20 ± 1.74	6.55 ± 0.93	6.01 ± 1.13	4.47 ± 1.45	2.92 ± 0.61	0.084
	$CD44^+/CD62L^+$ (T_{CM})	3.17 ± 0.12[a]	6.77 ± 0.52[b]	6.29 ± 0.28[b]	8.37 ± 1.07[b]	7.82 ± 0.68[b]	**< 0.001**
	$CD44^+/CD62L^-$ (T_{EM})	3.73 ± 0.62[a]	3.60 ± 0.34[a]	2.70 ± 0.31[a,b]	1.68 ± 0.25[b]	2.39 ± 0.21[a,b]	**0.005**
% of $CD8^+$ T cells	$CD69^+$	7.59 ± 0.80	8.20 ± 0.20	9.04 ± 0.29	7.46 ± 0.83	7.09 ± 0.27	0.156
	$CD25^+$	1.20 ± 0.28	1.97 ± 0.17	1.72 ± 0.18	1.96 ± 0.39	1.74 ± 0.05	0.203
	$CD44^-/CD62L^+$ (naïve)	89.3 ± 1.54	83.9 ± 1.27	84.3 ± 1.39	83.4 ± 2.90	86.6 ± 0.32	0.203
	$CD44^-/CD62L^-$ (effector)	5.83 ± 1.02	7.61 ± 0.91	6.72 ± 1.12	6.56 ± 2.00	4.13 ± 1.15	0.294
	$CD44^+/CD62L^+$ (T_{CM})	3.62 ± 0.29[a]	5.89 ± 0.71[a,b]	6.01 ± 0.45[a,b]	6.91 ± 0.69[b]	7.04 ± 0.85[b]	**0.008**
	$CD44^+/CD62L^-$ (T_{EM})	1.42 ± 0.30	2.70 ± 0.24	2.99 ± 0.37	3.39 ± 0.84	2.47 ± 0.31	0.119

One-way ANOVA or Kruskal-Wallis test. Labeled means at each time point without a shared letter are significantly different. n = 3–7/time point.

Consistent with tumor-infiltrating T_{CM} cells, the percentage of splenic $CD44^+/CD62L^+$ T_{CM} cells within $CD4^+$ and $CD8^+$ T cells was also increased over time. The distribution of other splenic effector and memory cell populations is shown in **Additional File 1: Table S3**.

4T1.2-HER2 tumor growth was associated with changes in tumor-infiltrating immune cells expressing effector molecules

To better understand the functional status of effector cells, we assessed the expression of effector molecules (IFNγ, IL-2, TNFα and perforin) within $CD4^+$, $CD8^+$ and $CD49b^+$ cells, respectively. Among tumor-infiltrating effector cells, there was a significant difference in the percentage of $IFN\gamma^+$ cells within $CD4^+$ T cells (Fig. 4A) (one-way ANOVA, $F(4, 20) = 2.961$, $p = 0.045$) across all time points. The percentage of $IFN\gamma^+$ cells within $CD8^+$ T cells (Fig. 4B) was unchanged over time, and the percentage of $IFN\gamma^+$ cells within $CD49b^+$ NK cells (Fig. 4C) (one-way ANOVA, $F(4, 20) = 17.83$, $p < 0.001$) was increased from D9 to D12 and reduced from D15 to D18. The percentage of $IL\text{-}2^+$ cells within $CD4^+$ T cells (Fig. 4D) (one-way ANOVA, $F(4, 20) = 37.97$, $p < 0.001$) was increased from D6 to D12 and reduced from D12 to D18, the percentage of $IL\text{-}2^+$ cells within $CD8^+$ T cells (Fig. 4E) (one-way ANOVA, $F(4, 20) = 43.71$, $p < 0.001$) was increased from D9 to D12 and reduced from D15 to D18, and the percentage of $IL\text{-}2^+$ cells within $CD49b^+$ NK cells (Fig. 4F) (Kruskal-Wallis test, $KW = 15.65$, $p = 0.004$) was reduced at D18. The percentage of $TNF\alpha^+$ cells within $CD4^+$ T cells (Fig. 4G) was not significantly changed over time, the percentage of $TNF\alpha^+$ cells within $CD8^+$ T cells (Fig. 4H) (one-way ANOVA, $F(4, 20) = 4.350$, $p = 0.011$) was reduced at D18 compared to D9, and the percentage of $TNF\alpha^+$ cells within $CD49b^+$ NK cells (Fig. 4I) (one-way ANOVA, $F(4, 20) = 7.442$, $p < 0.001$) was reduced at D15-18 compared to D6. The percentage of $perforin^+$ cells within $CD8^+$ T cells (Fig. 4J) (one-way ANOVA, $F(4, 20) = 6.278$, $p = 0.002$) was increased at D15 compared to D6, followed by a reduction at D18. The percentage of $perforin^+$ cells within $CD49b^+$ NK cells (Fig. 4K) (one-way ANOVA, $F(4, 20) = 5.852$, $p = 0.003$) was reduced at D18 compared to D9-12.

Among splenic effector cells, the percentage of $IFN\gamma^+$ cells and $IL\text{-}2^+$ cells within $CD4^+$ T cells, $CD8^+$ T cells and $CD49b^+$ NK cells, respectively, was increased from D6 to D15, followed by a reduction at D18 (**Additional File 2: Figure S5**). The percentage of $TNF\alpha^+$ cells within $CD4^+$ and $CD8^+$ T cells was increased from D6 to D9, and the percentage of $perforin^+$ cells within $CD8^+$ T cells and $CD49b^+$ NK cells was increased at D12-15 compared to D6 (**Additional File 2: Figure S5**).

4T1.2-HER2 tumor regression occurred concurrently with HER2-specific IFNγ production

To further characterize antigen-specific T cell response during the initial tumor growth and regression, we assessed IFNγ secretion by tumor-infiltrating (Table 2) and splenic (**Additional File 1: Table S4**) immune cells following *ex vivo* stimulation with an $H\text{-}2K^d$-restricted HER2 peptide, a control HA peptide, anti-CD3/anti-CD28 antibodies, or without stimulus, respectively. Differences between HER2 and HA peptide-stimulated groups at each time point were further assessed using paired t test or Wilcoxon test (a two-way ANOVA was not applicable due to non-normal distribution of the data) (Fig. 5 and **Additional File 2: Figure S6**). IFNγ secretion by tumor-infiltrating immune cells in HER2 group was higher than HA group at D12 (paired t test, $p = 0.030$) and D15 (Wilcoxon test, $p = 0.063$) (Fig. 5). IFNγ secretion by splenic immune cells in HER2 group was higher than HA group at D12 (Wilcoxon test, $p = 0.063$) (**Additional File 2: Figure S6**).

Table 2
Temporal changes in IFNγ secretion by tumor-infiltrating immune cells during 4T1.2-HER2 tumor growth.

Tumor	HER2	HA	αCD3 + αCD28	Media
D6	108.7 ± 71.78	96.84 ± 69.76	199800 ± 38625	75.78 ± 35.91
D9	60.84 ± 41.52	12.80 ± 8.564	196966 ± 73138	7.309 ± 7.309
D12	315.7 ± 148.3	13.61 ± 7.986	326294 ± 88817	29.09 ± 12.32
D15	319.7 ± 222.7	150.5 ± 139.3	135152 ± 50084	153.5 ± 136.7
D18	102.6 ± 90.46	45.64 ± 40.28	40855 ± 34650	40.79 ± 31.37
Data are expressed in pg/mL. n = 3–6/time point.				

Tumor volume during the second phase of 4T1.2-HER2 tumor growth was correlated with the density of tumor-infiltrating immune cells and the percentage of effector and immunosuppressive cells

In mice that demonstrated the second phase of 4T1.2-HER2 tumor growth (recurrence), tumor volume was not correlated with the number of total tumor-infiltrating immune cells (Fig. 6A) but was negatively correlated with the number of tumor-infiltrating immune cells per cm^3 of tumor (Fig. 6B) ($r = 0.662$, $p = 0.052$). In addition, tumor volume was not correlated with the percentage of tumor-infiltrating T cells (**Additional File 2: Figure S7**), but was positively correlated with the percentage of tumor-infiltrating $CD11b^+/Gr\text{-}1^+$ MDSCs (Fig. 6C) ($r = 0.842$, $p = 0.004$) and $CD11b^+/Ly6C^{lo}/Ly6G^+$ gMDSCs (Fig. 6D) ($r = 0.657$, $p = 0.055$), and negatively correlated with the percentage of tumor-infiltrating $CD11b^+/Ly6C^{hi}/Ly6G^-$ mMDSCs (Fig. 6E) ($r=-0.903$, $p < 0.001$), $CD4^+$:MDSC (Fig. 6F) ($r=-0.774$, $p = 0.014$) and $CD8^+$:MDSC (Fig. 6G) ($r=-0.776$, $p = 0.014$) ratios.

Additionally, during the second phase of tumor growth or tumor rejection, tumor volume was positively correlated with splenic cell number and the percentage of splenic MDSCs, and negatively correlated with the percentage of splenic effector cells (**Additional File 2: Figure S8**). Further, splenic effector to immunosuppressive cell ratios were significantly higher in mice that rejected the tumor compared to mice that demonstrated the second phase of tumor growth (**Additional File 2: Figure S9**).

Discussion

Preclinical cancer models that closely mimic human diseases are valuable tools to study cancer immune responses and develop immunotherapeutic strategies. In the current study, we comprehensively characterized host immune responses in the orthotopic 4T1.2-HER2 murine breast cancer model, which integrated a surrogate tumor antigen HER2 into the clinically relevant, yet poorly immunogenic 4T1.2 metastatic breast cancer model.

4T1.2 and 4T1.2-HER2 tumor cells had similar proliferation rates *in vitro*, suggesting that the addition of human HER2 protein to murine 4T1.2 tumor cells did not change cell-intrinsic pathways that regulate tumor cell proliferation. However, *in vivo* growth rates of orthotopic 4T1.2 and 4T1.2-HER2 tumors in immunocompetent BALB/c mice were drastically different. In contrast to the rapid, continuous tumor growth of the 4T1.2 tumor, 4T1.2-HER2 tumor demonstrated a short period of initial tumor growth followed by spontaneous tumor regression, indicating a critical role of host factors in controlling 4T1.2-HER2 tumor growth. In immunodeficient BALB/c *scid* mice, 4T1.2-HER2 tumor growth tracked the rapid, continuous growth pattern of the parental 4T1.2 model without spontaneous regression. These results suggest that the adaptive immune system plays an important role in 4T1.2-HER2 tumor control. Because the expression of MHC and co-stimulatory molecules was not different between 4T1.2 and 4T12-HER2 tumor cells, the involvement of adaptive immunity in 4T1.2-HER2 tumor control may be attributed to the expression of HER2 antigen. Interestingly, following 4T1.2-HER2 tumor regression in immunocompetent mice, a subset of mice demonstrated a second phase of tumor outgrowth, whereas the others completely rejected the tumor. Future studies are needed to better understand the host factors that contribute to the distinct outcomes of tumor recurrence vs. tumor rejection.

In both the spleen and the TME, the percentage of $CD4^+$ and $CD8^+$ T cells was inversely correlated with tumor volume and demonstrated a reduction during the initial tumor growth followed by an increase during tumor regression. However, a stepwise increase in the percentage of splenic and tumor-infiltrating dendritic cells ($CD11c^+$/I-Ad^+) was observed throughout the initial tumor growth and regression, suggesting that the immune system may be recognizing and responding to the 4T1.2-HER2 tumor soon after tumor inoculation. Moreover, there was a stepwise increase in the percentage of IFNγ $^+$, IL-2^+ and perforin$^+$ T cells and NK cells throughout the initial tumor growth and regression. An increase in splenic TNFα$^+$ T cells was also observed during the initial tumor growth. IFNγ production and cytotoxicity are the two most critical anti-tumor effector functions (2, 3, 32). IL-2 is produced by activated T cells and NK cells and promotes the activation, differentiation and cytotoxicity of effector cells (33, 34). TNFα is produced by both myeloid and lymphoid cells with pleiotropic effects, and T cell-derived TNFα has been shown to contribute to anti-tumor immunity (35–38). Therefore, the observed increase in effector cells expressing these molecules suggest that an anti-tumor immune response may be elicited upon tumor inoculation and mount up throughout tumor growth and regression. Further, *ex vivo* stimulation with an H-$2K^d$-restricted HER2 peptide induced HER2-specific IFNγ secretion, which peaked during the tumor regression phase at D12-15. When adjusting for cell number, the greatest HER2-specific IFNγ response was still observed at D12-15. Together, these data suggest that 4T1.2-HER2 tumor regression occurred concurrently with an increase in both the number and functional capacity of effector cells.

During an immune response to infection or cancer, activated T cells can further differentiate into memory cells to provide long-term protection. Memory T cells are categorized into two subsets, central memory (T_{CM}, $CD44^+$/$CD62L^+$/$CCR7^+$) and effector memory (T_{EM}, $CD44^+$/$CD62L^-$/$CCR7^-$) cells, with distinct localization patterns and functional capacity (39–42). Both T_{CM} and T_{EM} cells play important roles in host immunity, and T_{CM} cells have been shown to confer greater anti-tumor immunity compared to T_{EM}

cells when adoptively transferred into hosts (43–46). In the current study, we observed an increase in splenic and tumor-infiltrating $CD4^+$ and $CD8^+$ T_{CM} cells during tumor regression compared to the initial tumor growth period. This suggests that the anti-tumor immune response occurred concurrently with the formation of immunological memory, which may provide further protection.

Tumor progression or regression is a result of the interactions between various pro- and anti-tumor mediators. MDSCs are a major component of the immunosuppressive network in cancer. In the 4T1.2 mammary tumor model, tumor progression is associated with pronounced MDSC accumulation (21, 23). Consistently in the 4T1.2-HER2 model, we observed an increase in splenic and tumor-infiltrating MDSCs during the initial tumor growth, followed by a reduction during tumor regression. As a result, T cell to MDSC ratios decreased during the initial tumor growth and increased during tumor regression. These data suggest that at the beginning of 4T1.2-HER2 tumor development, pro-tumorigenic, immunosuppressive factors such as MDSCs dominated, resulting in the initial tumor growth. While at the same time, the immune system recognized the growing tumor and mounted an anti-tumor immune response with increased level of effector cells and greater antigen-specific responses, which eventually overcame the immunosuppression and resulted in tumor regression. Interestingly, other observations from our laboratory suggest that MDSC accumulation during 4T1.2-HER2 initial tumor growth and regression may be influenced by age and body weight. Furthermore, tumor progression during the second phase of 4T1.2-HER2 tumor growth was associated with a decrease in tumor immune infiltration and the domination of immunosuppressive cells over effector cells.

In human breast cancer, $HER2^+$ and TNBC subtypes are characterized by higher levels of T cell infiltration compared to HR^+ subtypes (9, 10), and T cell infiltration is negatively correlated with tumor recurrence and mortality in $HER2^+$ and TNBC (11–14). In contrast to T cells, circulating MDSC levels in breast cancer patients are positively correlated with clinical stage, metastatic tumor burden and treatment with chemotherapy (47–49). Few clinical studies have assessed MDSC infiltration into the TME. One study reports a significant expansion of MDSCs within breast tumors compared to normal breast tissue (50). Furthermore, MDSC infiltration is greater in the breast cancer tissue of TNBC patients compared to HR^+ breast cancer patients (51). Consistent with the observations in TNBC patients, the 4T1.2-HER2 model of TNBC induced significant T cell infiltration, and tumor progression and regression were associated with changes in the infiltration of effector and immunosuppressive cells into the TME. Therefore, the orthotopic 4T1.2-HER2 model presents a novel, clinically relevant model of TNBC to assess antigen-specific immune responses.

Conclusions

Results from the current study suggest that the integration of a surrogate tumor antigen, human HER2, into the clinically relevant, yet poorly immunogenic 4T1.2 metastatic breast cancer model enhanced its immunogenicity and induced antigen-specific immune responses. In contrast to the rapid, continuous tumor growth of the parental 4T1.2 model, 4T1.2-HER2 tumor growth demonstrated a spontaneous

regression period that is dependent on the adaptive immune system. Tumor regression occurred concurrently with an increase in the ratio of effector to immunosuppressive cells, the capacity of effector cells to produce cytokine and cytotoxic molecules, and importantly, HER2-specific immune response as indicated by IFNγ production. Therefore, the orthotopic 4T1.2-HER2 model could be a powerful tool to study the modulation of antigen-specific immune responses to chemotherapeutic, immunotherapeutic or novel therapeutic interventions to ultimately improve clinical outcomes in breast cancer patients.

Abbreviations

CTL: cytotoxic T cell; HER2: human epidermal growth factor receptor-2; IFNg: interferon gamma; IL-2: interleukin-2; MDSC: myeloid-derived suppressor cell; NK: natural killer; TAA: tumor-associated antigen; T_{CM}: central memory T cell; T_{EM}: effector memory T cell; TIL:, tumor-infiltrating lymphocyte; TME: tumor microenvironment; TNBC: triple-negative breast cancer; TNFa: tumor necrosis factor alpha; Treg: regulatory T cell.

Declarations

Availability of data and materials

The datasets used and/or analyzed during the current study are available from the corresponding author on reasonable request.

Competing interests

The authors declare that they have no competing interests.

Ethics approval and consent to participate

Institutional Animal Care and Use Committee approval of the study protocol was obtained prior to conducting the study. This study did not involve human subjects thus consent to participate is not relevant.

Consent for publication

Not applicable

Funding

This work was supported, in part, by the American Institute for Cancer Research (325117). Yitong Xu was supported by a T32 Training Program (T32GM108563) Research training in Physiological Adaptations to Stress while at the Pennsylvania State University (University Park, PA).

Authors' contributions

CJR and YX participated in the conception and design of the work, collection and assembly of data, data analysis and interpretation, and manuscript writing. All authors approved the manuscript for submission.

Acknowledgements

We thank the Flow Cytometry Facility in the Huck Institutes of the Life Sciences at the Pennsylvania State University (University Park, PA) for technical support of this project. Yitong Xu was supported by a T32 Training Program (T32GM108563) Research training in Physiological Adaptations to Stress while at the Pennsylvania State University (University Park, PA).

References

1. American Cancer Society. Cancer Facts & Figs. 2019.
2. Ostrand-Rosenberg S. Immune surveillance: a balance between protumor and antitumor immunity. Curr Opin Genet Dev. 2008;18(1):11–8.
3. Swann JB, Smyth MJ. Immune surveillance of tumors. J Clin Invest. 2007;117(5):1137–46.
4. Dunn GP, Old LJ, Schreiber RD. The three Es of cancer immunoediting. Annu Rev Immunol. 2004;22:329–60.
5. Lindau D, Gielen P, Kroesen M, Wesseling P, Adema GJ. The immunosuppressive tumour network: myeloid-derived suppressor cells, regulatory T cells and natural killer T cells. Immunology. 2013;138(2):105–15.
6. Bonaventura P, Shekarian T, Alcazer V, Valladeau-Guilemond J, Valsesia-Wittmann S, Amigorena S, et al. Cold Tumors: A Therapeutic Challenge for Immunotherapy. Front Immunol. 2019;10:168.
7. Duan Q, Zhang H, Zheng J, Zhang L. Turning Cold into Hot: Firing up the Tumor Microenvironment. Trends Cancer. 2020;6(7):605–18.
8. Gatti-Mays ME, Balko JM, Gameiro SR, Bear HD, Prabhakaran S, Fukui J, et al. If we build it they will come: targeting the immune response to breast cancer. NPJ Breast Cancer. 2019;5:37.
9. Adams S, Gatti-Mays ME, Kalinsky K, Korde LA, Sharon E, Amiri-Kordestani L, et al. Current Landscape of Immunotherapy in Breast Cancer: A Review. JAMA Oncol. 2019.
10. Diana A, Carlino F, Franzese E, Oikonomidou O, Criscitiello C, De Vita F, et al. Early Triple Negative Breast Cancer: Conventional Treatment and Emerging Therapeutic Landscapes. Cancers (Basel). 2020;12(4).

11. Denkert C, von Minckwitz G, Darb-Esfahani S, Lederer B, Heppner BI, Weber KE, et al. Tumour-infiltrating lymphocytes and prognosis in different subtypes of breast cancer: a pooled analysis of 3771 patients treated with neoadjuvant therapy. Lancet Oncol. 2018;19(1):40–50.
12. Kovacs A, Stenmark Tullberg A, Werner Ronnerman E, Holmberg E, Hartman L, Sjostrom M, et al. Effect of Radiotherapy After Breast-Conserving Surgery Depending on the Presence of Tumor-Infiltrating Lymphocytes: A Long-Term Follow-Up of the SweBCG91RT Randomized Trial. J Clin Oncol. 2019;37(14):1179–87.
13. Loi S, Drubay D, Adams S, Pruneri G, Francis PA, Lacroix-Triki M, et al. Tumor-Infiltrating Lymphocytes and Prognosis: A Pooled Individual Patient Analysis of Early-Stage Triple-Negative Breast Cancers. J Clin Oncol. 2019;37(7):559–69.
14. Park JH, Jonas SF, Bataillon G, Criscitiello C, Salgado R, Loi S, et al. Prognostic value of tumor-infiltrating lymphocytes in patients with early-stage triple-negative breast cancers (TNBC) who did not receive adjuvant chemotherapy. Ann Oncol. 2019;30(12):1941–9.
15. Pardoll DM. The blockade of immune checkpoints in cancer immunotherapy. Nat Rev Cancer. 2012;12(4):252–64.
16. Emens LA. Breast Cancer Immunotherapy: Facts and Hopes. Clin Cancer Res. 2018;24(3):511–20.
17. Keenan TE, Tolaney SM. Role of Immunotherapy in Triple-Negative Breast Cancer. J Natl Compr Canc Netw. 2020;18(4):479–89.
18. Hegde PS, Chen DS. Top 10 Challenges in Cancer Immunotherapy. Immunity. 2020;52(1):17–35.
19. Schoenfeld AJ, Hellmann MD. Acquired Resistance to Immune Checkpoint Inhibitors. Cancer Cell. 2020;37(4):443–55.
20. van Elsas MJ, van Hall T, van der Burg SH. Future Challenges in Cancer Resistance to Immunotherapy. Cancers (Basel). 2020;12(4).
21. Cao Y, Slaney CY, Bidwell BN, Parker BS, Johnstone CN, Rautela J, et al. BMP4 inhibits breast cancer metastasis by blocking myeloid-derived suppressor cell activity. Cancer Res. 2014;74(18):5091–102.
22. Eckhardt BL, Parker BS, van Laar RK, Restall CM, Natoli AL, Tavaria MD, et al. Genomic analysis of a spontaneous model of breast cancer metastasis to bone reveals a role for the extracellular matrix. Mol Cancer Res. 2005;3(1):1–13.
23. Turbitt WJ, Xu Y, Sosnoski DM, Collins SD, Meng H, Mastro AM, et al. Physical Activity Plus Energy Restriction Prevents 4T1.2 Mammary Tumor Progression, MDSC Accumulation, and an Immunosuppressive Tumor Microenvironment. Cancer prevention research (Philadelphia, Pa). 2019;12(8):493–506.
24. Helguera G, Rodriguez JA, Penichet ML. Cytokines fused to antibodies and their combinations as therapeutic agents against different peritoneal HER2/neu expressing tumors. Mol Cancer Ther. 2006;5(4):1029–40.
25. Li P, Yang L, Li T, Bin S, Sun B, Huang Y, et al. The Third Generation Anti-HER2 Chimeric Antigen Receptor Mouse T Cells Alone or Together With Anti-PD1 Antibody Inhibits the Growth of Mouse

Breast Tumor Cells Expressing HER2 in vitro and in Immune Competent Mice. Front Oncol. 2020;10:1143.

26. Nilofar Danishmalik S, Lee SH, Sin JI. Tumor regression is mediated via the induction of HER263-71-specific CD8 + CTL activity in a 4T1.2/HER2 tumor model: no involvement of CD80 in tumor control. Oncotarget. 2017;8(16):26771–88.
27. Shanker A, Pellom ST Jr, Dudimah DF, Thounaojam MC, de Kluyver RL, Brooks AD, et al. Bortezomib Improves Adoptive T-cell Therapy by Sensitizing Cancer Cells to FasL Cytotoxicity. Cancer Res. 2015;75(24):5260–72.
28. Kershaw MH, Jackson JT, Haynes NM, Teng MW, Moeller M, Hayakawa Y, et al. Gene-engineered T cells as a superior adjuvant therapy for metastatic cancer. J Immunol. 2004;173(3):2143–50.
29. Choong K, Ammori J, Hamzeh K, Graor H, Kim J. Tumor-Draining Lymph Nodes Contain Immunodominant Peptide-Specific T Cells which Demonstrate Efficacy in Murine Models of Adoptive Immunotherapy. Journal of Nature Science (JNSCI). 2017;3(6):398.
30. Nagata Y, Furugen R, Hiasa A, Ikeda H, Ohta N, Furukawa K, et al. Peptides derived from a wild-type murine proto-oncogene c-erbB-2/HER2/neu can induce CTL and tumor suppression in syngeneic hosts. J Immunol. 1997;159(3):1336–43.
31. Piechocki MP, Pilon SA, Wei WZ. Complementary antitumor immunity induced by plasmid DNA encoding secreted and cytoplasmic human ErbB-2. J Immunol. 2001;167(6):3367–74.
32. Dunn GP, Old LJ, Schreiber RD. The immunobiology of cancer immunosurveillance and immunoediting. Immunity. 2004;21(2):137–48.
33. Jiang T, Zhou C, Ren S. Role of IL-2 in cancer immunotherapy. Oncoimmunology. 2016;5(6):e1163462.
34. Liao W, Lin JX, Leonard WJ. Interleukin-2 at the crossroads of effector responses, tolerance, and immunotherapy. Immunity. 2013;38(1):13–25.
35. Deng L, Liang H, Burnette B, Beckett M, Darga T, Weichselbaum RR, et al. Irradiation and anti-PD-L1 treatment synergistically promote antitumor immunity in mice. J Clin Invest. 2014;124(2):687–95.
36. Habtetsion T, Ding ZC, Pi W, Li T, Lu C, Chen T, et al. Alteration of Tumor Metabolism by CD4 + T Cells Leads to TNF-alpha-Dependent Intensification of Oxidative Stress and Tumor Cell Death. Cell Metab. 2018;28(2):228–42. e6.
37. Josephs SF, Ichim TE, Prince SM, Kesari S, Marincola FM, Escobedo AR, et al. Unleashing endogenous TNF-alpha as a cancer immunotherapeutic. J Transl Med. 2018;16(1):242.
38. Kearney CJ, Vervoort SJ, Hogg SJ, Ramsbottom KM, Freeman AJ, Lalaoui N, et al. Tumor immune evasion arises through loss of TNF sensitivity. Sci Immunol. 2018;3(23).
39. Golubovskaya V, Wu L. Different Subsets of T Cells, Memory, Effector Functions, and CAR-T Immunotherapy. Cancers (Basel). 2016;8(3).
40. Martin MD, Badovinac VP. Defining Memory CD8 T Cell. Front Immunol. 2018;9:2692.

41. Sckisel GD, Mirsoian A, Minnar CM, Crittenden M, Curti B, Chen JQ, et al. Differential phenotypes of memory CD4 and CD8 T cells in the spleen and peripheral tissues following immunostimulatory therapy. J Immunother Cancer. 2017;5:33.
42. van Faassen H, Saldanha M, Gilbertson D, Dudani R, Krishnan L, Sad S. Reducing the stimulation of CD8 + T cells during infection with intracellular bacteria promotes differentiation primarily into a central (CD62LhighCD44high) subset. J Immunol. 2005;174(9):5341–50.
43. Berger C, Jensen MC, Lansdorp PM, Gough M, Elliott C, Riddell SR. Adoptive transfer of effector CD8 + T cells derived from central memory cells establishes persistent T cell memory in primates. J Clin Invest. 2008;118(1):294–305.
44. Klebanoff CA, Finkelstein SE, Surman DR, Lichtman MK, Gattinoni L, Theoret MR, et al. IL-15 enhances the in vivo antitumor activity of tumor-reactive CD8 + T cells. Proc Natl Acad Sci U S A. 2004;101(7):1969–74.
45. Klebanoff CA, Gattinoni L, Torabi-Parizi P, Kerstann K, Cardones AR, Finkelstein SE, et al. Central memory self/tumor-reactive CD8 + T cells confer superior antitumor immunity compared with effector memory T cells. Proc Natl Acad Sci U S A. 2005;102(27):9571–6.
46. Wang X, Berger C, Wong CW, Forman SJ, Riddell SR, Jensen MC. Engraftment of human central memory-derived effector CD8 + T cells in immunodeficient mice. Blood. 2011;117(6):1888–98.
47. Bergenfelz C, Larsson AM, von Stedingk K, Gruvberger-Saal S, Aaltonen K, Jansson S, et al. Systemic Monocytic-MDSCs Are Generated from Monocytes and Correlate with Disease Progression in Breast Cancer Patients. PLoS One. 2015;10(5):e0127028.
48. Diaz-Montero CM, Salem ML, Nishimura MI, Garrett-Mayer E, Cole DJ, Montero AJ. Increased circulating myeloid-derived suppressor cells correlate with clinical cancer stage, metastatic tumor burden, and doxorubicin-cyclophosphamide chemotherapy. Cancer Immunol Immunother. 2009;58(1):49–59.
49. Safarzadeh E, Hashemzadeh S, Duijf PHG, Mansoori B, Khaze V, Mohammadi A, et al. Circulating myeloid-derived suppressor cells: An independent prognostic factor in patients with breast cancer. J Cell Physiol. 2019;234(4):3515–25.
50. Toor SM, Syed Khaja AS, El Salhat H, Faour I, Kanbar J, Quadri AA, et al. Myeloid cells in circulation and tumor microenvironment of breast cancer patients. Cancer Immunol Immunother. 2017;66(6):753–64.
51. Kumar S, Wilkes DW, Samuel N, Blanco MA, Nayak A, Alicea-Torres K, et al. DeltaNp63-driven recruitment of myeloid-derived suppressor cells promotes metastasis in triple-negative breast cancer. J Clin Invest. 2018;128(11):5095–109.

Figures

Figure 1

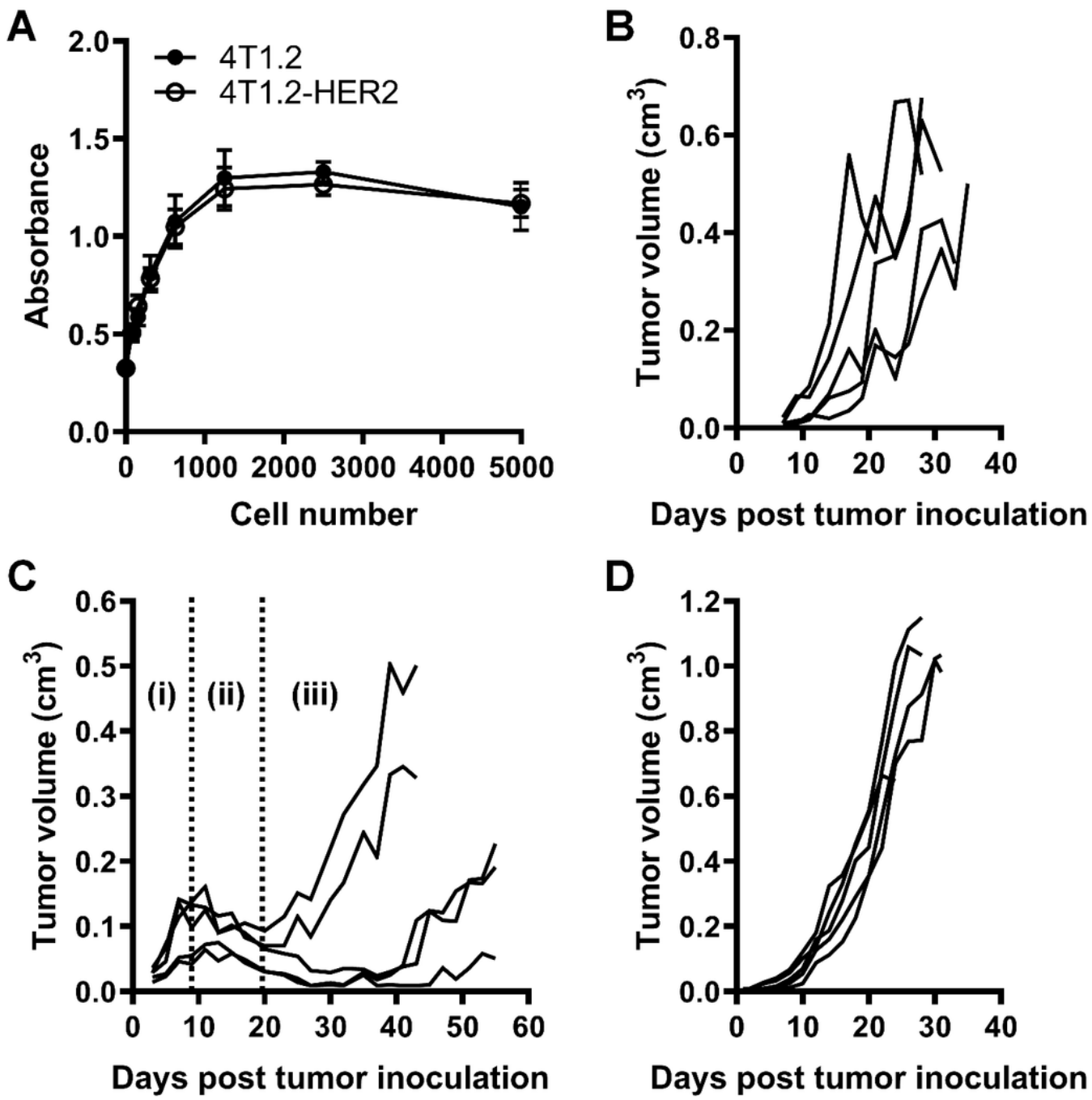

Figure 1

In vitro and in vivo proliferation rates of 4T1.2 and 4T1.2-HER2 tumor cells. (A) In vitro proliferation rates were similar between 4T1.2 and 4T1.2-HER2 cells as determined by MTS proliferation assay. The experiments were repeated four times and summary data were shown. (B-D) In vivo tumor growth of individual mice. Compared to the rapid, continuous progression of 4T1.2 tumor (5x104 cells inoculated) in wildtype BALB/c mice (n=5) (B), 4T1.2-HER2 (2x106 cells inoculated) tumor growth in wildtype BALB/c

mice (n=4) (C) consisted of three phases: (i) initial tumor growth, (ii) spontaneous tumor regression, and (iii) a second phase of tumor outgrowth or tumor rejection. (D) In immunodeficient BALB/c scid mice (n=5), 4T1.2-HER2 tumor (5x105 cells inoculated) demonstrated a rapid, continuous progression with no spontaneous regression phase.

Figure 2

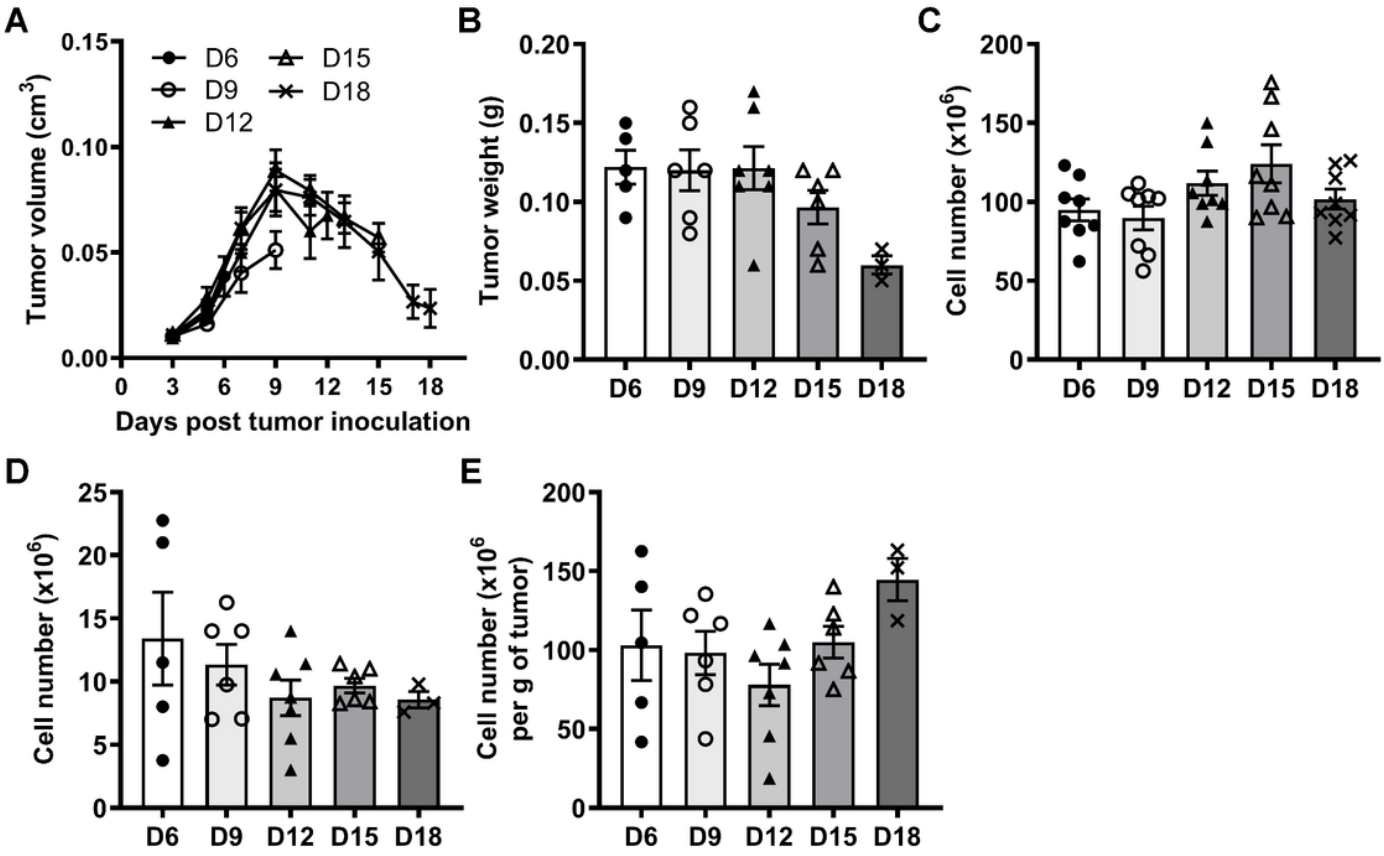

Figure 2

4T1.2-HER2 tumor growth and regression, temporal pattern of splenic and tumor-infiltrating immune cells. Female BALB/c mice were orthotopically inoculated with 2x106 4T1.2-HER2 tumor cells and sacrificed at D6, 9, 12, 15 and 18 post tumor inoculation (n=8/time point). Primary tumor growth of mice in each time point group (A). There was a significant difference in terminal tumor weight (B) (one-way ANOVA, $F(4,22)=3.167$, $p=0.034$) and splenic cell number (C) (one-way ANOVA, $F(4,35)=2.692$, $p=0.047$) across all time points. The number of total tumor-infiltrating immune cells (D) and infiltrating cells per gram of tumor (E) was not significantly different across all time points.

Figure 3

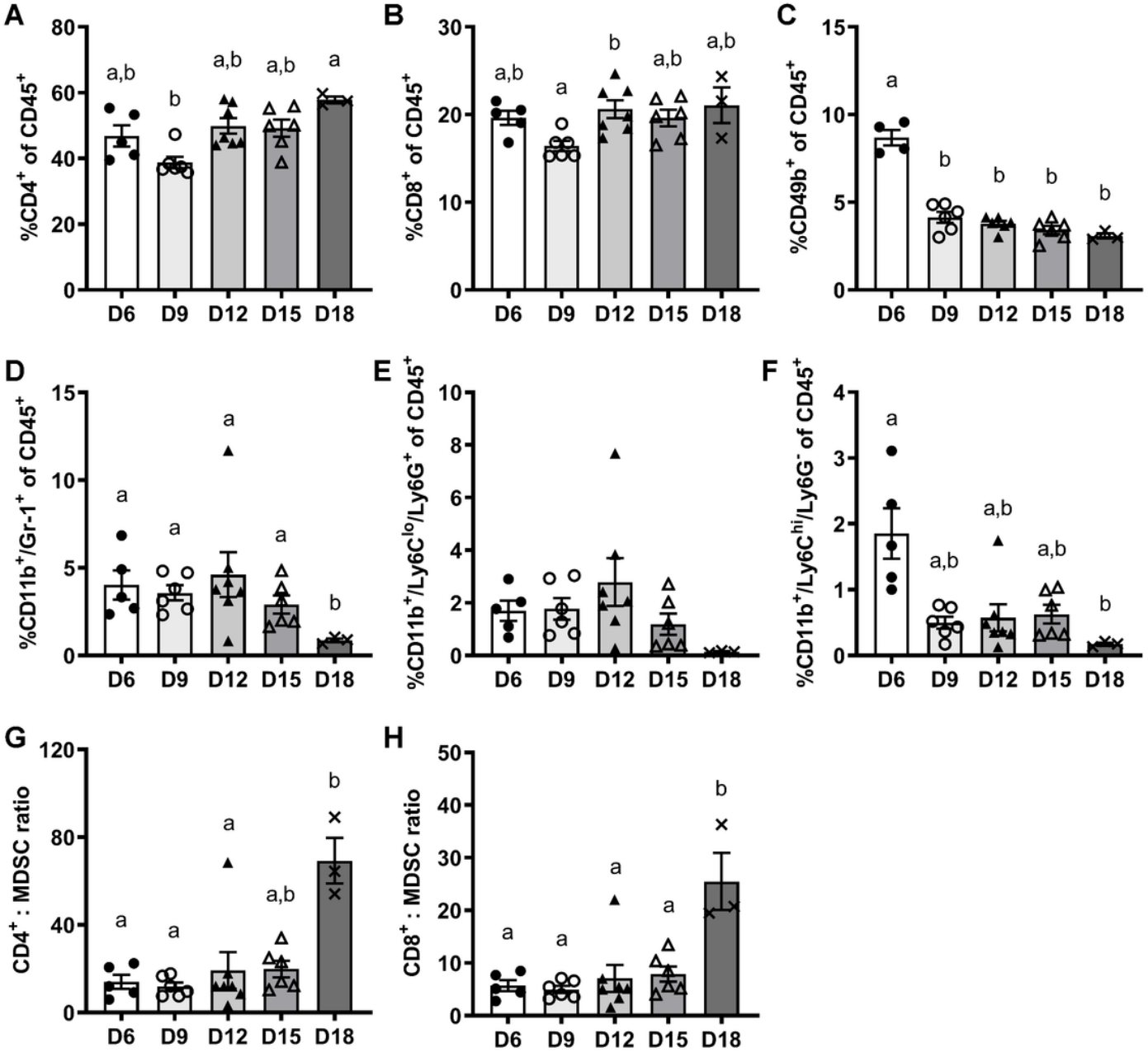

Figure 3

4T1.2-HER2 tumor growth was associated with changes in tumor-infiltrating effector and immunosuppressive cells. The percentage of tumor-infiltrating CD4+ (A) (Kruskal-Wallis test, KW=14.35, p=0.006) and CD8+ (B) (one-way ANOVA, F(4,22)=3.35, p=0.028) T cells was reduced from D6 to D9 and increased after D9. The percentage of tumor-infiltrating CD49b+ NK cells (C) (one-way ANOVA, F(4,20)=55.01, p<0.001) was reduced at D9-18 compared to D6. The percentage of tumor-infiltrating Gr-1+/CD11b+ MDSCs (D) (one-way ANOVA, F(4,22)=4.962, p=0.005) was reduced at D18, CD11b+/Ly6Clo/Ly6G+ gMDSCs (E) was unchanged, and CD11b+/Ly6Chi/Ly6G- mMDSCs (F) (Kruskal-

Wallis test, KW=13.79, p=0.008) was reduced over time. Tumor-infiltrating CD4+:MDSC (G) (one-way ANOVA, F(4,22)=5.168, p=0.004) and CD8+:MDSC (H) (one-way ANOVA, F(4,22)=5.481, p=0.003) ratios were increased at D18. Labeled means at each time point without a shared letter are significantly different. n=3-7/time point.

Figure 4

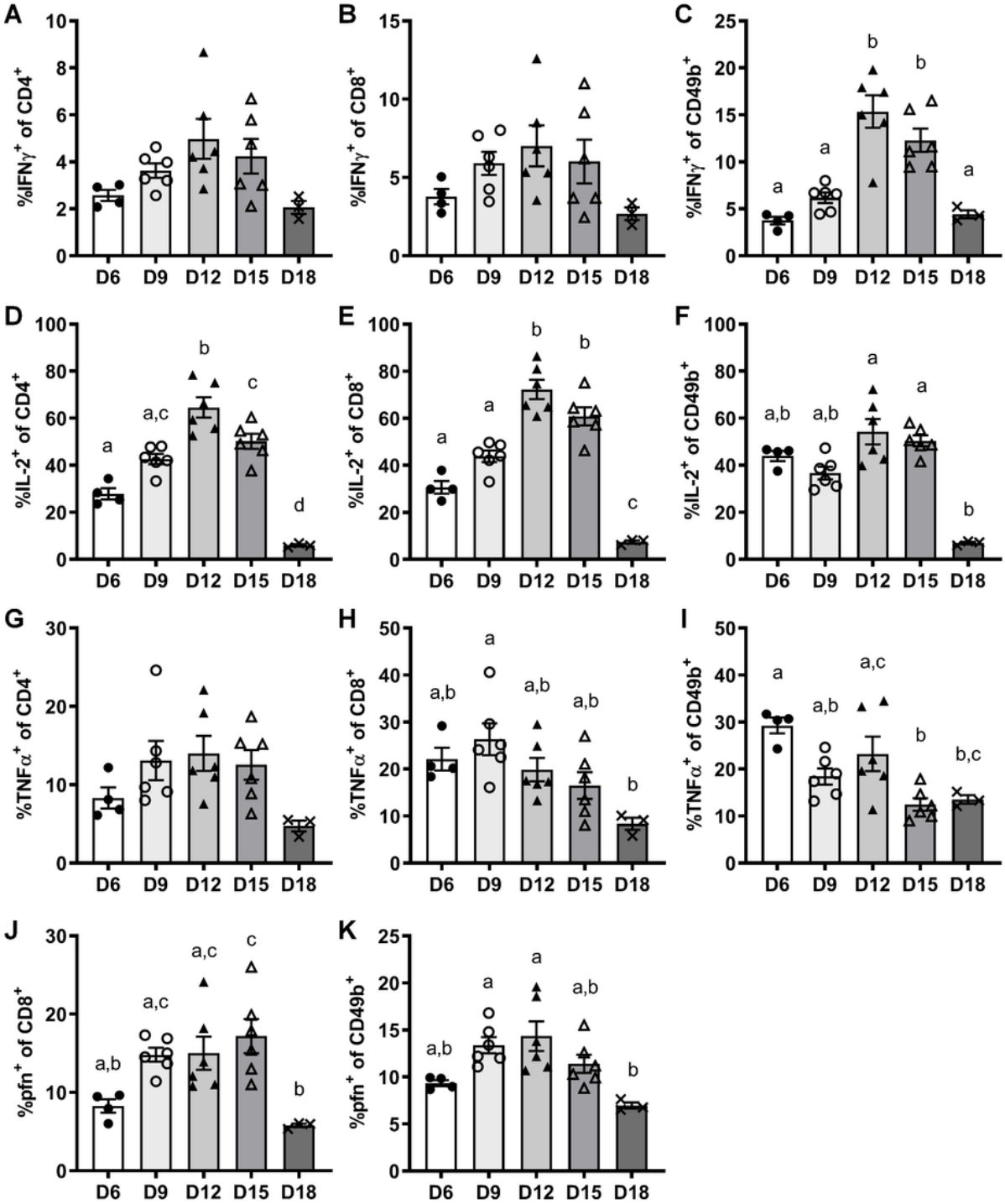

Figure 4

4T1.2-HER2 tumor growth was associated with changes in tumor-infiltrating immune cells expressing effector molecules. At sacrifice, tumor-infiltrating immune cells were isolated and incubated with brefeldin A (BFA) or DMSO control for 4h at 37°C, followed by flow cytometric analysis of effector molecules within CD4+, CD8+ and CD49b+ cells, respectively. Results from cells incubated with BFA were shown. There was a significant difference in the percentage of IFNγ+ cells within CD4+ T cells (A) ($F(4,20)=2.961$, $p=0.045$) across all time points. The percentage of IFNγ+ cells within CD8+ T cells (B) was unchanged over time, and the percentage of IFNγ+ cells within CD49b+ NK cells (C) ($F(4,20)=17.83$, $p<0.001$) was increased from D9 to D12 and reduced from D15 to D18. The percentage of IL-2+ cells within CD4+ T cells (D) ($F(4,20)=37.97$, $p<0.001$) was increased from D6 to D12 and reduced from D12 to D18, the percentage of IL-2+ cells within CD8+ T cells (E) ($F(4,20)=43.71$, $p<0.001$) was increased from D9 to D12 and reduced from D15 to D18, and the percentage of IL-2+ cells within CD49b+ NK cells (F) ($KW=15.65$, $p=0.004$) was reduced at D18. The percentage of TNFα+ cells within CD4+ T cells (G) was not significantly changed over time, the percentage of TNFα+ cells within CD8+ T cells (H) ($F(4,20)=4.350$, $p=0.011$) was reduced at D18 compared to D9, and the percentage of TNFα+ cells within CD49b+ NK cells (I) ($F(4,20)=7.442$, $p<0.001$) was reduced at D15-18 compared to D6. The percentage of perforin+ cells within CD8+ T cells (J) ($F(4,20)=6.278$, $p=0.002$) was increased at D15 compared to D6, followed by a reduction at D18. The percentage of perforin+ cells within CD49b+ NK cells (K) ($F(4,20)=5.852$, $p=0.003$) was reduced at D18 compared to D9-12. One-way ANOVA (A-E, G-K) or Kruskal-Wallis test (F). Labeled means at each time point without a shared letter are significantly different. n=3-6/time point.

Figure 5

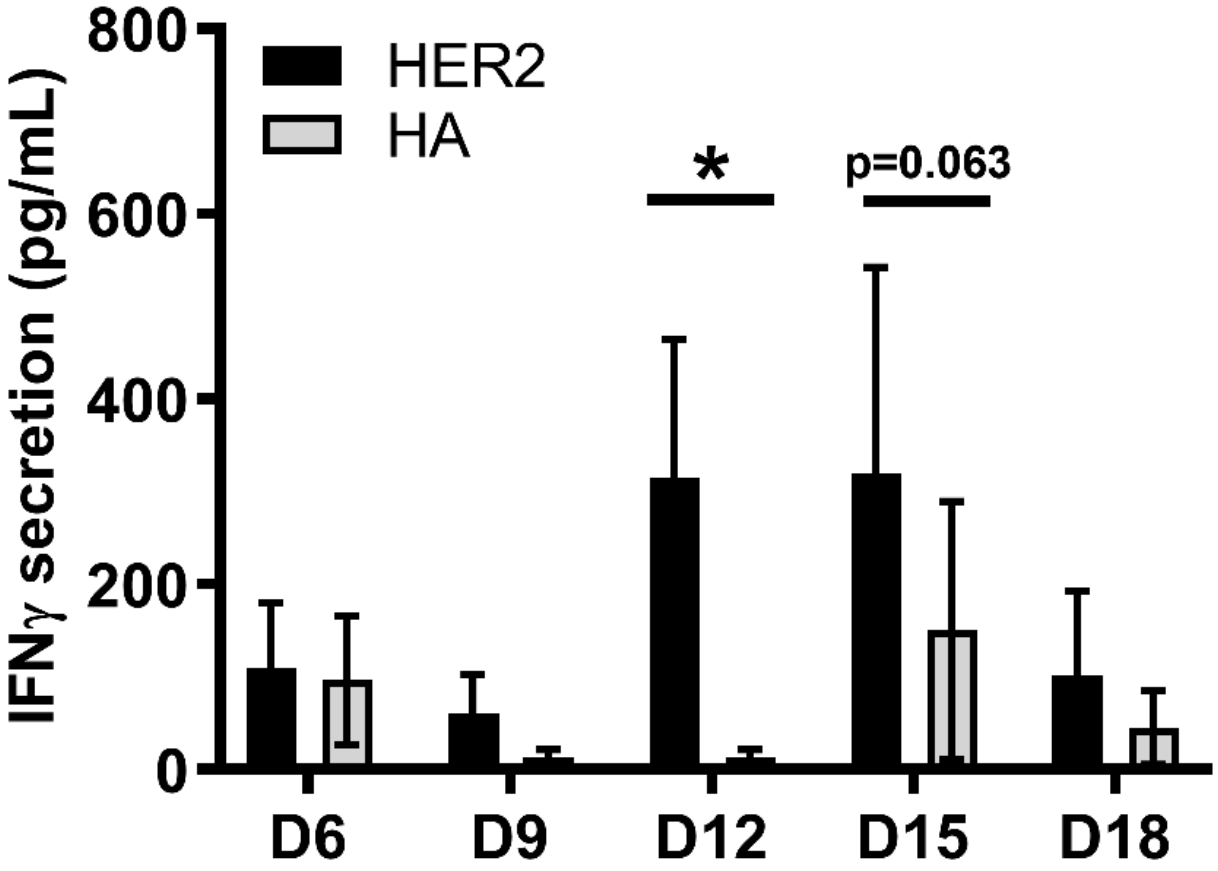

Figure 5

4T1.2-HER2 tumor regression occurred concurrently with HER2-specific IFNγ production by tumor-infiltrating immune cells. 4T1.2-HER2 tumor-bearing mice were sacrificed at day 6, 9, 12, 15 and 18 post tumor inoculation (n=3-6/time point). Tumor-infiltrating immune cells were stimulated with 10 μg/mL HER2 p63-71 peptide, 10 μg/mL HA p518-526 peptide, 1 μg/mL anti-CD3 plus anti-CD28 (positive control), or cultured without stimulus (negative control) for 48h, and IFNγ secretion in the culture supernatants was analyzed by ELISA. Results from HER2 and HA stimulation groups were shown. IFNγ secretion by tumor-infiltrating immune cells was higher in HER2 group than HA group at D12 and D15. Differences between HER2 and HA groups at each time point were assessed using paired t test or Wilcoxon test. *$p<0.05$.

Figure 6

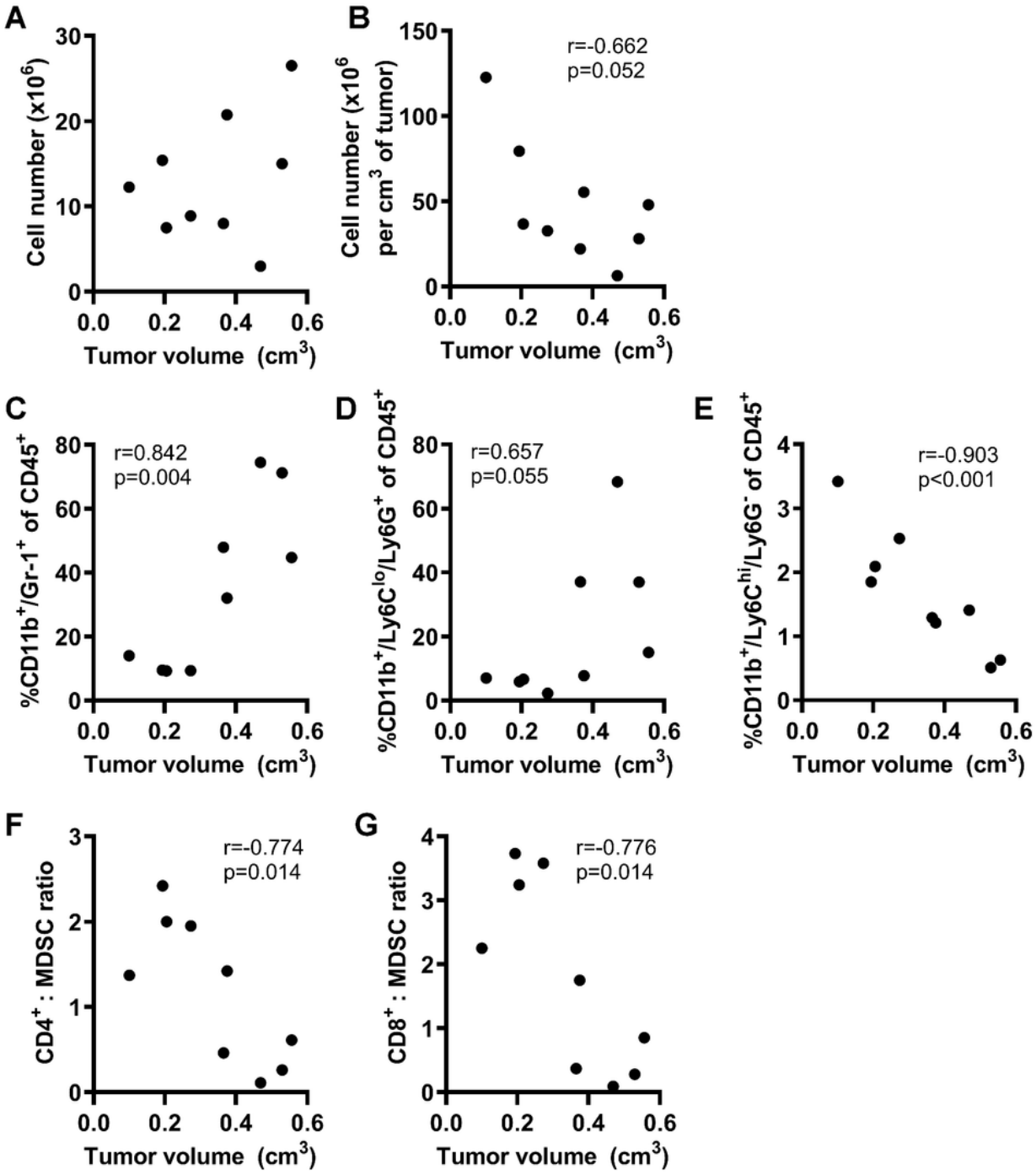

Figure 6

Tumor volume during the second phase of tumor growth was correlated with tumor-infiltrating immune cells. Mice inoculated with 4T1.2-HER2 tumor cells were maintained until the second phase of tumor growth (recurrence) or complete rejection, and tumor-bearing mice (n=10) were sacrificed between day 44-56 post tumor inoculation. Tumor volume was not correlated with the number of total tumor-infiltrating immune cells (A), but was negatively correlated with the number of tumor-infiltrating immune cells per

cm3 of tumor (B) (r=0.662, p=0.052). In addition, tumor volume was positively correlated with the percentage of tumor-infiltrating CD11b+/Gr-1+ MDSCs (C) (r=0.842, p=0.004) and CD11b+/Ly6Clo/Ly6G+ gMDSCs (D) (r=0.657, p=0.055), and negatively correlated with the percentage of tumor-infiltrating CD11b+/Ly6Chi/Ly6G- mMDSCs (E) (r=-0.903, p<0.001), CD4+:MDSC (F) (r=-0.774, p=0.014) and CD8+:MDSC (G) (r=-0.776, p=0.014) ratios. Pearson correlation test.

Supplementary Files

This is a list of supplementary files associated with this preprint. Click to download.

- Additionalfile1.pdf
- Additionalfile2.pdf